ACS APPLIED ELECTRONIC MATERIALS

pubs.acs.org/acsaelm Letter

# Enhanced Photoresponse in Few-Layer $SnS_2$ Field-Effect Transistors Modified with Methylammonium Lead Iodide Perovskite

Michael J. Loes, Alexey Lipatov, Nataliia S. Vorobeva, Haidong Lu, Jehad Abourahma, Dmitry S. Muratov, Alexei Gruverman, and Alexander Sinitskii*

Cite This: *ACS Appl. Electron. Mater.* 2023, 5, 705−713 Read Online

ACCESS | Metrics & More | Article Recommendations | Supporting Information

**ABSTRACT:** We demonstrate that decoration with methylammonium lead iodide perovskite ($MAPbI_3$) nanoparticles is an efficient approach to engineer strong visible light photoresponse in electronic devices based on two-dimensional (2D) materials with limited optical absorptivity. This approach was demonstrated using 2D $SnS_2$, a promising electronic material with a band gap of about 2.3 eV and poor absorption in the visible range of spectrum. Field-effect transistors based on pristine 2D $SnS_2$ show an n-type transport with high on−off ratios. Decoration with isolated $MAPbI_3$ nanoparticles qualitatively retains the transfer characteristics of the devices but dramatically increases their photoresponse in the entire visible range of the spectrum. In particular, the photoresponse of the $MAPbI_3$-decorated devices to the red light is entirely engineered by the perovskite modification of $SnS_2$, which by itself does not absorb in the red region of the spectrum. The $MAPbI_3$-decorated $SnS_2$ devices exhibit stable, reproducible photoswitching over numerous cycles with response times of no longer than 12 ms. An analysis of a $MAPbI_3$−$SnS_2$ heterostructure by Kelvin probe force microscopy resulted in an energy level diagram suggesting a transfer of the photoexcited electrons in $MAPbI_3$ to the conduction band of the n-type $SnS_2$ channel. The photoresponse characteristics of the perovskite-modified $SnS_2$ devices were shown to be consistent with the intrinsic optical properties of $MAPbI_3$. The described perovskite decoration approach should be applicable to engineering photoresponse in a variety of other devices based on 2D electronic materials with low optical absorptivity.

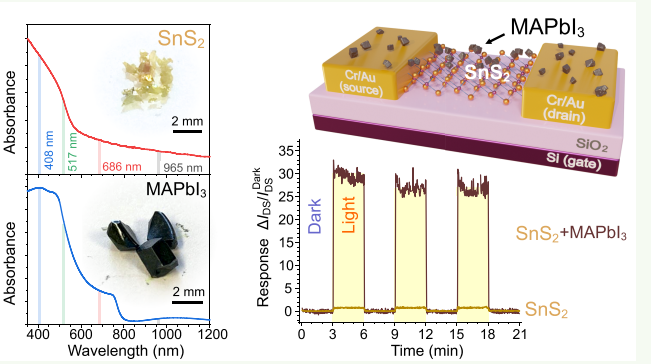


**KEYWORDS:** *2D materials, tin disulfide, methylammonium lead iodide, heterostructure, photoresponse, Kelvin probe force microscopy*



Over the past decade, two-dimensional (2D) crystals and hybrid halide perovskites have been two of the most actively researched classes of materials, especially for electronic and optoelectronic applications.[1−3] In recent studies, it has been shown that some of the complementary properties of these materials can be utilized in heterostructural devices with enhanced properties.[4−17] For example, heterostructures of 2D materials and hybrid perovskites offer many advantages for visible-range photodetectors.[4−15] On one hand, 2D materials offer a great diversity of electronic properties and can be conveniently patterned into planar device structures. On the other hand, a perovskite layer deposited on a device channel can provide high visible light absorptivity and long electron−hole diffusion lengths,[3] enhancing the light−matter interactions. In previous studies, it was shown that hybrid halide perovskite layers enhance photoresponses in devices based on 2D transition-metal chalcogenides (TMCs), such as $MoS_2$, $WS_2$, and $WSe_2$.[4−15] However, these materials have electronic band gaps in the near-infrared region and could exhibit visible light photoresponse without a perovskite overlayer, which was exploited in numerous studies.[1,18,19] In this work, we extend the idea of perovskite decoration to 2D electronic materials with larger band gaps that do not absorb light through most of the visible range of spectrum and thus would not be naturally considered for optical photodetectors.

Tin disulfide ($SnS_2$) is an example of a 2D material with a limited light absorptivity in the visible range of spectrum due to the band gap of about 2.3 eV.[20−22] $SnS_2$ has a layered $CdI_2$-type crystal structure[20] (space group $P\bar{3}m1$) that is shown in Figure 1a.[23] High-quality $SnS_2$ crystals can be conveniently grown by a direct reaction between metallic tin and sulfur vapor at about 700 °C; see the detailed description of the synthesis of $SnS_2$ in the Supporting Information. A representative Raman spectrum of a few-layer $SnS_2$ shows the out-of-plane $A_{1g}$ vibrational mode at 314.3 $cm^{-1}$, which is

**Received:** July 20, 2022
**Accepted:** January 5, 2023
**Published:** February 6, 2023

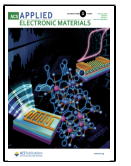

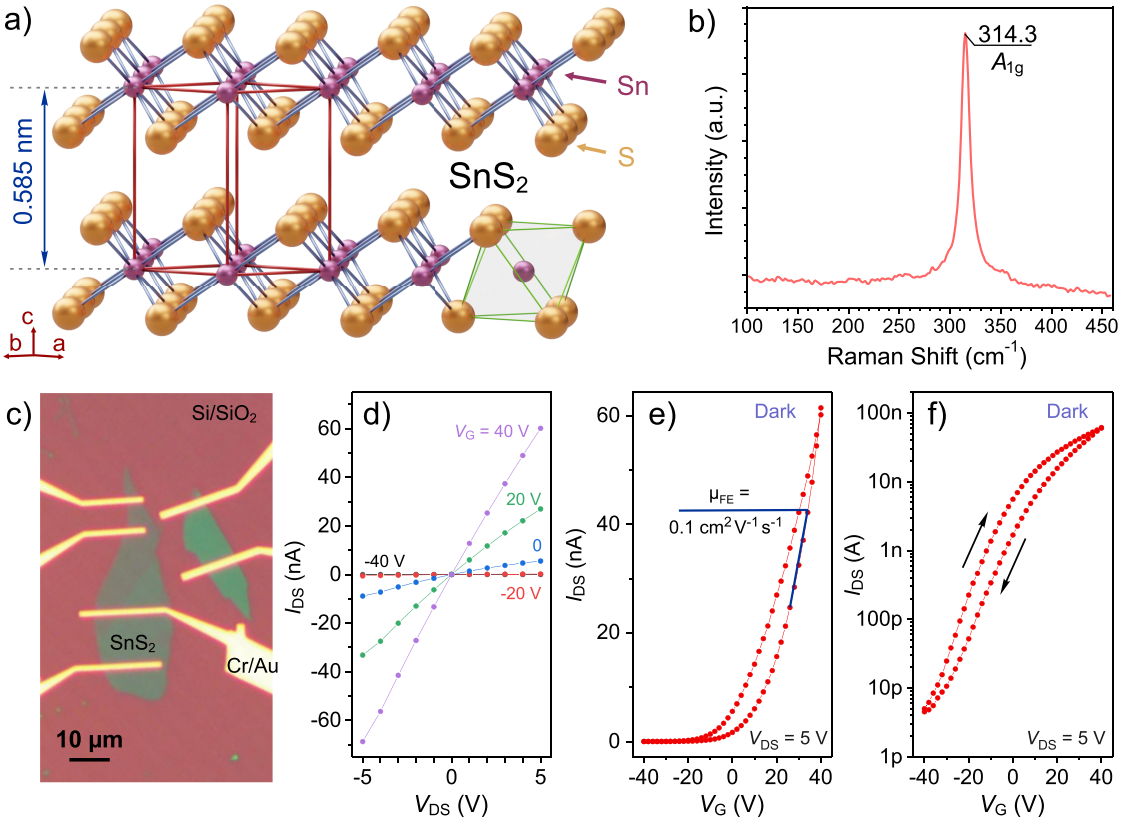


**Figure 1.** Structural and electronic properties of $SnS_2$. (a) Crystal structure of $SnS_2$. The red lines indicate the unit cell, while the green lines show the octahedral coordination of tin. (b) Representative Raman spectrum of few-layer $SnS_2$. (c) Optical photograph of $SnS_2$ devices fabricated on a $Si/SiO_2$ substrate. (d) $I_{DS}-V_{DS}$ dependences for a $SnS_2$ device measured in a vacuum at different gate voltages ($V_G$) ranging from −40 to 40 V. (e, f) $I_{DS}-V_G$ dependences at $V_{DS}$ = 5 V shown in linear (e) and logarithmic (f) current scales.

consistent with other spectra of $SnS_2$ in the literature.[21,22,24,25] $SnS_2$ was recently recognized as a promising electronic material with some of its electronic properties summarized in Figure 1c–f. The layered $SnS_2$ crystals can be conveniently exfoliated into monolayer and few-layer flakes using the conventional adhesive tape approach, and then these flakes can be patterned into electronic devices using the standard electron beam lithography (EBL). Figure 1c shows the optical photograph of field-effect transistor (FET) devices, in which thin $SnS_2$ flakes deposited on a $Si/SiO_2$ substrate bridge Cr(5 nm)/Au(20 nm) leads, which served as source (S) and drain (D) electrodes in the transport measurements. The conductive p-type Si separated from the $SnS_2$ device channels by a 300 nm thick layer of $SiO_2$ served as a global gate (G). Figure 1d shows that $SnS_2$ forms good contacts with Cr/Au electrodes, which can be seen from the linearity of the drain–source current ($I_{DS}$)/drain–source voltage ($V_{DS}$) dependences. The $I_{DS}-V_G$ characteristics that are shown in the linear and logarithmic $I_{DS}$ scales demonstrate that the $SnS_2$ devices exhibit an n-type semiconductor behavior with electron mobility of about 0.1 $cm^2\ V^{-1}\ s^{-1}$ (Figure 1e) and transistor on–off ratios $>10^4$ (Figure 1f); these values are comparable to similar back-gated, few-layer $SnS_2$ devices produced by mechanical exfoliation.[22,26,27] It should be noted that while this is a modest mobility compared to the more popular TMCs, such as $MoS_2$,[18] or $TiS_3$,[28] mobilities reaching 200 $cm^2\ V^{-1}\ s^{-1}$ have been reported for solution-gated $SnS_2$ devices,[20] demonstrating their potential for electronic applications.

The low visible light absorptivity of $SnS_2$ is illustrated by Figure 2a. The inset in Figure 2a shows optical photograph of the $SnS_2$ crystals prepared in this study, which are semi-transparent yellow flakes (also see Figure S1 in the Supporting Information). The spectrum in Figure 2a shows that these crystals do not absorb light in the red range of spectrum, and the absorption starts only as the photon energy increases into the green/blue range. The absorption edge of $SnS_2$ can be estimated from these data to rise at 565 nm (2.19 eV), in agreement with reported literature values of ~2.18–2.44 eV.[21] Below the band gap energy of $SnS_2$, minimal absorbance is seen; however, absorption increases sharply for incident photons with wavelengths below about 550 nm. In order to enhance the light–matter interactions in the $SnS_2$ devices, we modified them with methylammonium lead iodide ($MAPbI_3$), the optical properties of which are presented in Figure 2b. The bulk $MAPbI_3$ crystals are shown in the inset of Figure 2b, and unlike $SnS_2$, they are black and nontransparent. The spectrum in Figure 2b demonstrates that $MAPbI_3$ exhibits a strong optical absorption in the entire visible range of spectrum and has an absorption edge at about 795 nm (1.56 eV), which is in agreement with the previous studies.[29] Therefore, decoration of the $SnS_2$ FET channels with $MAPbI_3$ is expected to enhance the light–matter interactions throughout the entire visible range of spectrum and, in particular, enable the device photoresponse in the red region, where $SnS_2$ does not absorb light because of its ~2.3 eV band gap.

The decoration of $SnS_2$ FETs with $MAPbI_3$ is illustrated by Figure 2c–h with a detailed device fabrication procedure


https://doi.org/10.1021/acsaelm.2c00947
ACS Appl. Electron. Mater. 2023, 5, 705–713

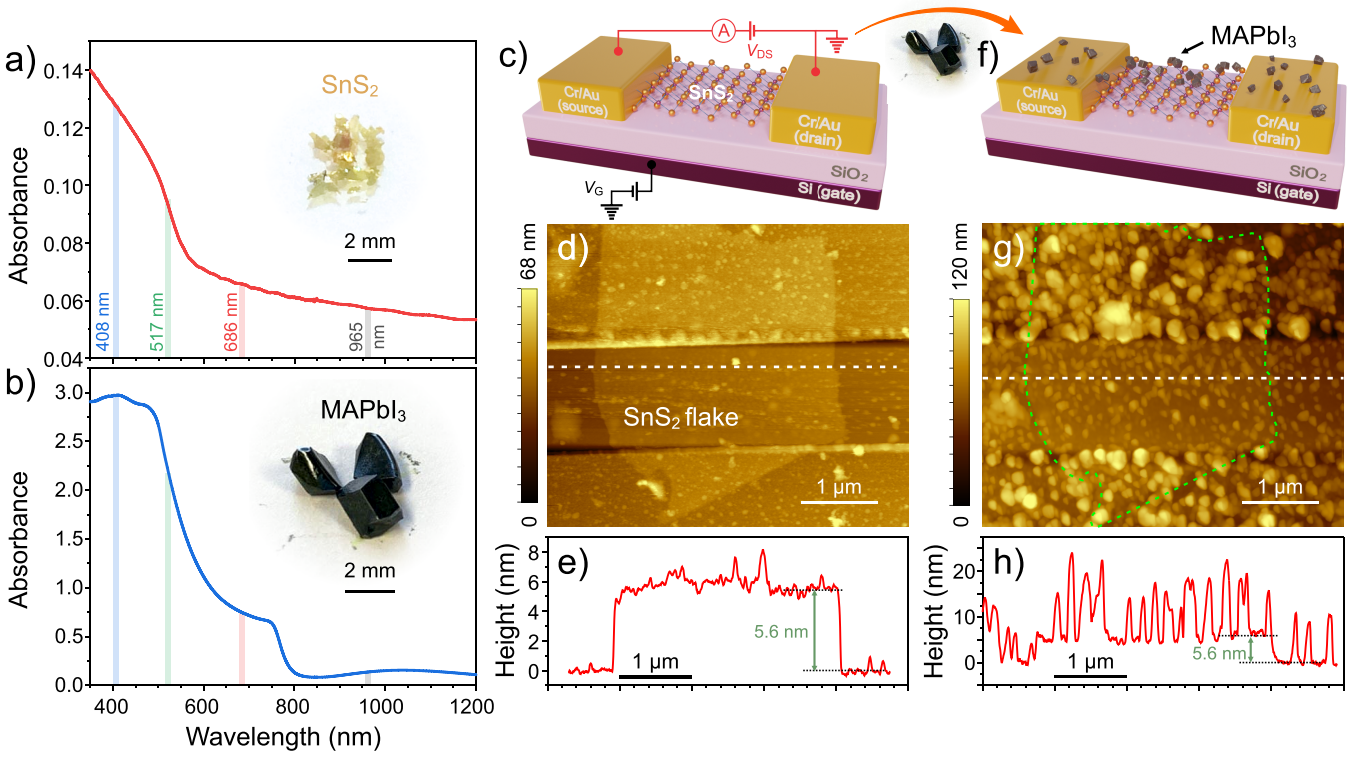


**Figure 2.** Decoration of $SnS_2$ devices with $MAPbI_3$ nanoparticles. (a, b) UV−vis−NIR absorption spectra of $SnS_2$ (a) and $MAPbI_3$ (b). The insets demonstrate optical photographs of the samples. The vertical lines show the wavelengths of the lasers that were used in this study.(c) Scheme of a $SnS_2$ FET. (d) AFM image of a representative $SnS_2$ FET that was used in this study. (e) AFM height profile measured across the $SnS_2$ flake shown in panel d; the measurement was taken along the dashed white line. (f) Scheme of a $SnS_2$ FET decorated with $MAPbI_3$ nanoparticles. (g) AFM image of the same $SnS_2$ device as in panel d after its decoration with $MAPbI_3$ nanoparticles. The dashed green line shows the contour of the $SnS_2$ flake. (h) AFM height profile measured across the perovskite-decorated $SnS_2$ flake shown in panel g; the measurement was taken along the dashed white line.

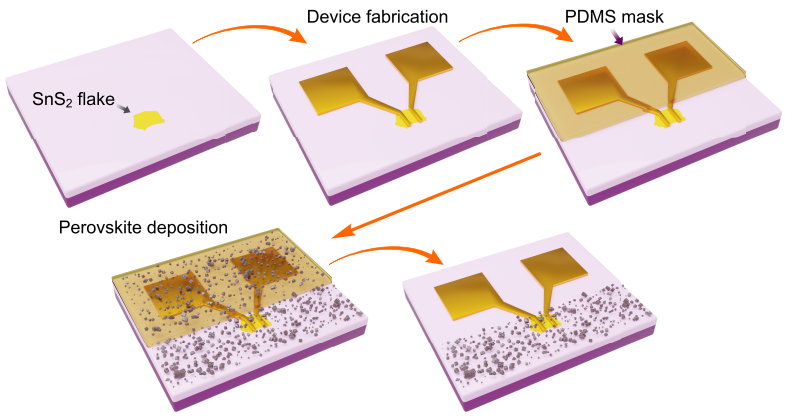


**Figure 3.** Scheme of fabrication of $MAPbI_3$-decorated $SnS_2$ devices. See text for details.

shown in Figure 3. Figure 2d demonstrates an atomic force microscopy (AFM) image of a representative FET device fabricated from a single $SnS_2$ flake. The height profile measured across this flake (Figure 2e) shows the thickness of about 5.6 nm, suggesting several layers of $SnS_2$. The device channel contains several foreign particles, which may be residues of either the adhesive tape used for the mechanical exfoliation of $SnS_2$ crystals or the EBL resist. In either case, these particles did not affect the electrical properties of this FET, which behaved similar to other previously reported $SnS_2$ devices,[20,22,26,27] as shown in Figure 4. It should be noted that these particles are not intrinsic to the fabrication process, as illustrated by Figure S2, which shows AFM images of two other as-prepared $SnS_2$ devices with much less surface contamination. Although one of the $SnS_2$ flakes in Figure S2 has a nearly perfect triangular shape, which is reminiscent of TMC crystals grown by chemical vapor deposition,[30,31] it was produced by mechanical exfoliation, just like other flakes in this study.

The deposition of $MAPbI_3$ on the devices was performed using the antisolvent-assisted spin-coating procedure.[29,32] After protection of gold electrodes with a thin layer of poly-dimethylsiloxane (PDMS), the $Si/SiO_2$ substrate with the devices was flooded with a solution of $CH_3NH_3I$ and $PbI_2$



https://doi.org/10.1021/acsaelm.2c00947
ACS Appl. Electron. Mater. 2023, 5, 705−713

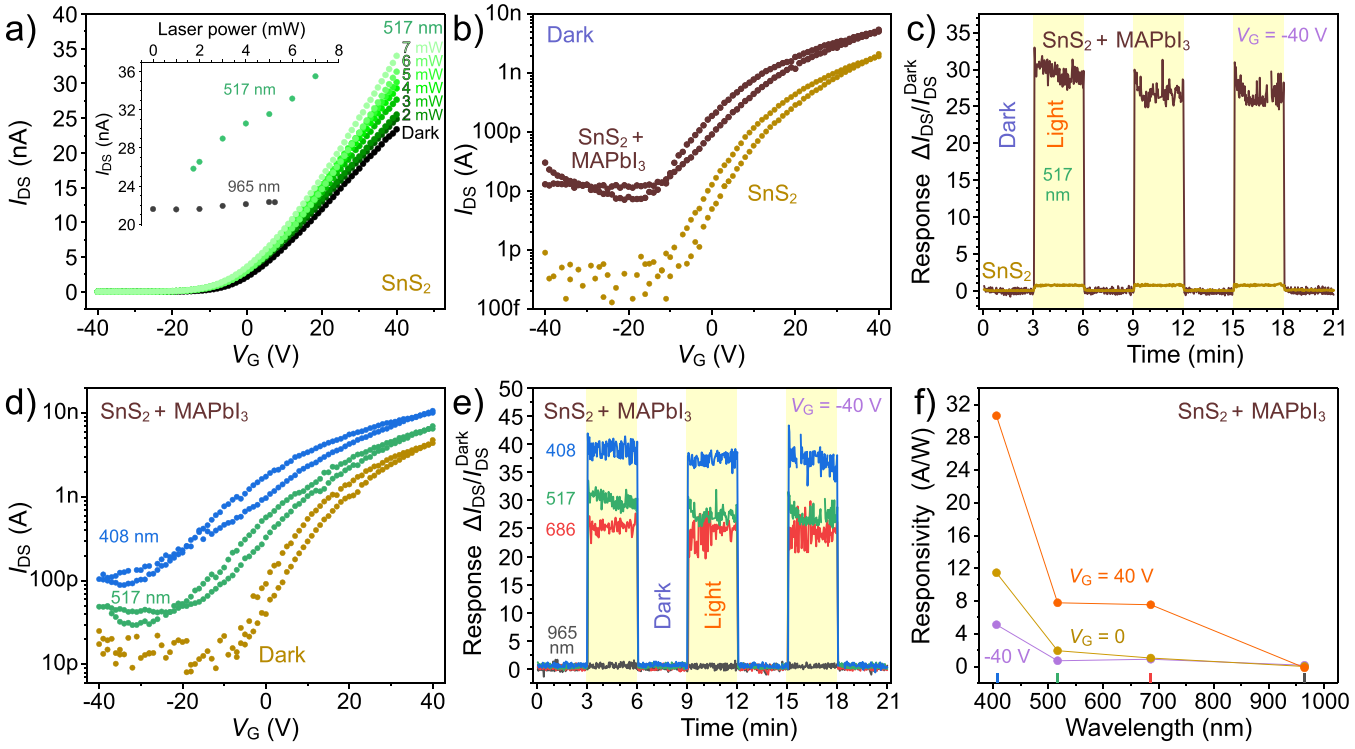


**Figure 4.** Optoelectronic characterization of $MAPbI_3$-decorated $SnS_2$ devices. (a) $I_{DS}-V_G$ dependences for a pristine $SnS_2$ device measured under illumination with a green laser (517 nm) at powers ranging from 0 to 7 mW. $V_{DS}$ = 0.1 V. The inset shows the dependences of $I_{DS}$ at $V_G$ = 40 V on the laser power for green (517 nm) and IR (965 nm) lasers. (b) $I_{DS}-V_G$ dependences measured in the dark for a $SnS_2$ device before and after the perovskite decoration. (c) Photoresponses of pristine and perovskite-decorated $SnS_2$ devices to excitation with a green laser measured at $V_G$ = −40 V and $V_{DS}$ = 0.1 V. (d) $I_{DS}-V_G$ dependences for a $MAPbI_3$-decorated $SnS_2$ device measured in the dark and under illumination with green (517 nm) and blue (408 nm) lasers. $V_{DS}$ = 0.1 V. (e) Photoresponses of a $MAPbI_3$-decorated $SnS_2$ device to excitation with blue (408 nm), green (517 nm), red (686 nm), and IR (965 nm) lasers measured at $V_G$ = −40 V and $V_{DS}$ = 0.1 V. (f) Photoresponsivity of a $MAPbI_3$-decorated $SnS_2$ device as a function of the excitation laser wavelength and the gate voltage. All data are shown for the device presented in Figure 2g.

powders in dimethylformamide (DMF) and dimethyl sulfoxide (DMSO) and then spin-coated at 3000 rpm for 30 s. About 5 s before the spinning cycle was finished, an antisolvent, such as ethyl acetate, was dripped over the substrate, which was then annealed at 60 °C for 10 min. During the annealing, the film darkens from transparent yellow to opaque black, indicating the formation of the $MAPbI_3$ perovskite structure.[29,33] Thin films on transparent substrates reveal the material to be deep maroon red; however, the material absorbs so strongly in the visible region[34] that on $Si/SiO_2$ substrates used in this work the film appears black (see Figure S3). The results of the X-ray diffraction (XRD) characterization of the perovskite material are also presented in Figure S3 along with their Rietveld refinement.

As shown schematically in Figure 2f, the reported procedure resulted in the formation of isolated $MAPbI_3$ nanoparticles on $SnS_2$ rather than a continuous perovskite film. This is important for understanding the electronic properties of the resulting $SnS_2$-$MAPbI_3$ devices. Because $MAPbI_3$ did not form a percolating layer, there was no alternative continuous conductive channel formed in parallel to the $SnS_2$ flake, and the transfer characteristics of the decorated devices were qualitatively the same as before the decoration. On the other hand, the perovskite nanoparticles on $SnS_2$ channels can be excited by visible light and increase photoresponsivity of the devices. It should be noted that even in the case of bulk TMCs that have high optical absorption coefficients,[35] the ultrathin devices made from these materials often exhibit low absolute absorbances because of the small thicknesses of the device channels.[2,36] Therefore, it has become a common practice to decorate the 2D devices with quantum dots, plasmonic nanoparticles, or other materials[2,36,37] to aid in absorption while still preserving the fundamental electrical properties of the underlying 2D channels.

Figure 2g shows AFM image of the same $SnS_2$ device as in Figure 2d after the perovskite modification. The isolated $MAPbI_3$ nanoparticles are clearly seen in the AFM image and in the representative height profile across the perovskite-decorated $SnS_2$ flake (Figure 2h). The 5.6 nm height of the $SnS_2$ flake can be identified in the height profile; relative to this height the perovskite nanoparticles were about 5−15 nm thick. Interestingly, the AFM image shows that $MAPbI_3$ particles have grown larger on Cr/Au contacts than on the $SnS_2$ flake or the bare $Si/SiO_2$ substrate, suggesting a greater affinity of the perovskite material to gold than to the sulfide or oxide surfaces. A rougher surface of Au electrodes compared to flat $SnS_2$ and $Si/SiO_2$ may also be beneficial for $MAPbI_3$ nucleation and crystallization.

The tendency of $MAPbI_3$ to densely cover gold electrodes was the reason we protected them with PDMS masks when the perovskite was deposited on $SnS_2$ devices (see Figure 3). In a typical device fabrication process, a $SnS_2$ flake was first exfoliated by the conventional adhesive tape method onto $Si/SiO_2$ and then used for electrode patterning by EBL, as described in the Supporting Information. Then, the Cr/Au contacts were covered with a protective PDMS mask, as shown



https://doi.org/10.1021/acsaelm.2c00947
ACS Appl. Electron. Mater. 2023, 5, 705−713

in Figure 3, so that only the device channel area remained exposed for the perovskite deposition. After the spin-coating of the solution of $CH_3NH_3I$ and $PbI_2$ and the formation of the perovskite particles, the PDMS mask was removed (see Figure 3). This procedure prevented the unnecessary formation of $MAPbI_3$ on the large Cr/Au pads, which were later contacted with the tips of a probe station in electrical measurements, and also ensured that no conductive bridges of a perovskite material could accidentally form between the electrodes outside the observed channel area. It should also be noted that because in this process the perovskite material is formed after a lithography process and in the contact area between the substrate and the PDMS mask, the deposition dynamics is different from that of the solution spin-coating on a bare $Si/SiO_2$. In our control experiments, we found that a significantly larger amount of the perovskite material would be deposited on an oxygen plasma-cleaned $Si/SiO_2$ substrate without devices, lithography residues, and PDMS masks using the same spin-coating process.

Electronic properties of $SnS_2$ devices before and after the perovskite decoration were measured at room temperature in a vacuum probe station at a base pressure of about $2 \times 10^{-6}$ Torr. The vacuum measurements were expected to minimize the doping effect of the surface adsorbates, such as water and oxygen, on the measured electronic properties of semiconducting materials[38] as well as to preserve the decoration of devices with $MAPbI_3$, which is known to degrade in ambient conditions. At the same time, because some degradation of $MAPbI_3$ was reported to occur over time even in a vacuum,[39] we performed all electrical characterization of perovskite-decorated $SnS_2$ devices within several days after the evacuation. The devices, while remained in a vacuum, were illuminated through a transparent window in a probe station chamber with infrared (IR, 965 nm), red (686 nm), green (517 nm), or blue (408 nm) lasers; the experimental setup is also discussed in our previous works.[40−42] These lasers provided us with two sets of data points below the band gap of pristine $SnS_2$ and two sets above. After the perovskite decoration, 965 nm remains below the band gap of $MAPbI_3$, with the remaining three sets above.

Figure 4 demonstrates the effect of perovskite decoration on the optoelectronic properties of $SnS_2$ devices. A drain−source voltage of 0.1 V was used for all of these measurements. Figure 4a shows that the pristine $SnS_2$ devices exhibit a photoresponse to an excitation with a green laser (517 nm), which has an energy greater than the band gap of $SnS_2$. The drain−source current ($I_{DS}$) increases in the entire tested range of gate voltages ($V_G$) from −40 to 40 V under the green light illumination, and the increase is proportional to the laser power. The linear dependence of the $I_{DS}$ at $V_G$ = 40 V on the power of a green laser is illustrated by the inset in Figure 4a. Correspondingly, the pristine devices exhibit negligible response to an IR laser with an energy smaller than the band gap of $SnS_2$ (see the inset in Figure 4a). This slight response to the 965 nm radiation is not without precedent[27,43] and has been attributed to virtual energy levels introduced within the band gap by defect states[27] including sulfur vacancies[35,44] and other traps that may lie at the interface between the conductive channel and the gate dielectric.[2] Transitions by low-energy photons from these defect-induced states to the conduction band can also contribute to this negligible photocurrent.[27] It is still clear that the response to radiation with energy above the band gap is far more effective for generating excited electrons.

The effect of perovskite decoration on the transfer characteristics of a $SnS_2$ device measured in the dark is illustrated by Figure 4b. As demonstrated previously, the pristine $SnS_2$ exhibits an n-type semiconducting behavior with on−off ratios of several orders of magnitude in field-effect electrical measurements.[20,22,26,27] Upon decoration with $MAPbI_3$ perovskite nanoparticles, the $I_{DS}$ current increases across the entire $V_G$ range, but the overall shape of the $I_{DS}-V_G$ dependence remains qualitatively the same. Thus, the decoration of a 2D $SnS_2$ device channel, while dramatically increasing the photoresponse of a device, as shown in the following panels, qualitatively retains its original transfer characteristics. The increase in the dark current of the device upon its decoration with $MAPbI_3$ could be caused by the local parallel conductions paths formed by perovskite nanoparticles on top of the $SnS_2$ channel (even though no global contact-to-contact percolation was evident, based on the AFM results).

The dramatically increased photoresponse of the $MAPbI_3$-decorated $SnS_2$ devices is illustrated by Figure 4c. Here, the photoresponse is presented as the relative change in the device current, $\text{Response} = (I_{DS}^{Light} - I_{DS}^{Dark})/I_{DS}^{Dark}$, where $I_{DS}^{Dark}$ and $I_{DS}^{Light}$ are drain−source currents measured at the same $V_{DS}$ and $V_G$ (in this case, $V_{DS}$ = 0.1 V and $V_G$ = −40 V) in the dark and under illumination, respectively. The photoresponse to the green laser (517 nm) increases by about 2 orders of magnitude after the decoration of a device with $MAPbI_3$ nanoparticles. Figure 4c also shows the reproducibility of the photoswitching in both pristine and perovskite-modified $SnS_2$ devices. Similar data obtained with other lasers used in this study can be found in Figure S4.

For three of the lasers used in this experiment, red (686 nm), green (517 nm), and blue (408 nm), that had energies sufficiently high to photoexcite electrons in $MAPbI_3$, the responses of the perovskite-modified devices increased with the laser energy, as illustrated by Figure 4d,e. This can be explained by the optical spectrum of $MAPbI_3$ presented in Figure 2b, which shows the increasing absorption of the perovskite from red to green to blue regions of spectrum. Correspondingly, the transfer characteristics of the $MAPbI_3$-decorated $SnS_2$ device in Figure 4d show the larger $I_{DS}$ increase across the entire $V_G$ range for the blue laser illumination compared to the green laser. A similar idea is conveyed by the photoswitching data presented in Figure 4e, which show the largest photoresponse of the $MAPbI_3$-decorated $SnS_2$ device to the blue laser and smaller photoresponses to the green and red lasers, in accordance with the optical absorption spectrum of $MAPbI_3$ shown in Figure 2b. The appreciable photocurrent in the $MAPbI_3$-decorated device under the red laser (686 nm) illumination is notable because its energy is smaller than the band gap of $SnS_2$, which means that this photoresponse is entirely engineered by the perovskite decoration and would not be expected in a pristine device. Furthermore, the IR (965 nm) laser did not produce any significant photoresponse in the device, which is consistent with the fact that its energy is smaller than the band gaps of both $SnS_2$ (Figure 2a) and $MAPbI_3$ (Figure 2b).

The photoresponse of these devices depends not only on the energy of the excitation light but also on the gate voltage, which can be deduced from Figure 4d. This idea is further conveyed by Figure 4f, which characterizes the device by a different metric, responsivity, which is a measure of the absolute photocurrent generated in a device per unit incident


https://doi.org/10.1021/acsaelm.2c00947
ACS Appl. Electron. Mater. 2023, 5, 705−713

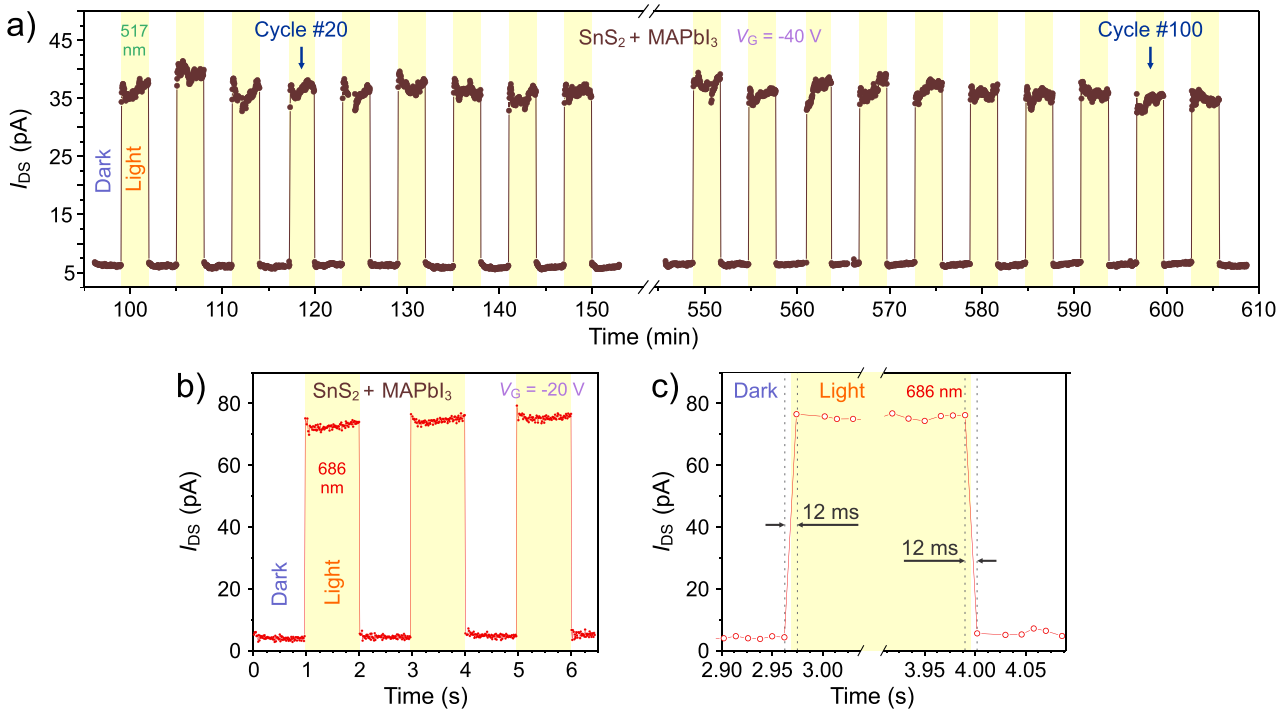


**Figure 5.** Functional characteristics of $MAPbI_3$−$SnS_2$ photodetectors. (a) Cyclic photoresponse of a perovskite-decorated $SnS_2$ device measured at $V_G$ = −40 V and $V_{DS}$ = 0.1 V. The device was repeatedly illuminated with a green laser. (b, c) Switching time measurements: (b) three cycles of photoresponse of a perovskite-decorated $SnS_2$ device to excitation with a red laser measured at $V_G$ = −20 V and $V_{DS}$ = 1 V and (c) zoomed-in second switching cycle from panel b, showing the rise and fall response times of about 12 ms. The data are shown for the device presented in Figure S2a after its modification with perovskite nanoparticles.

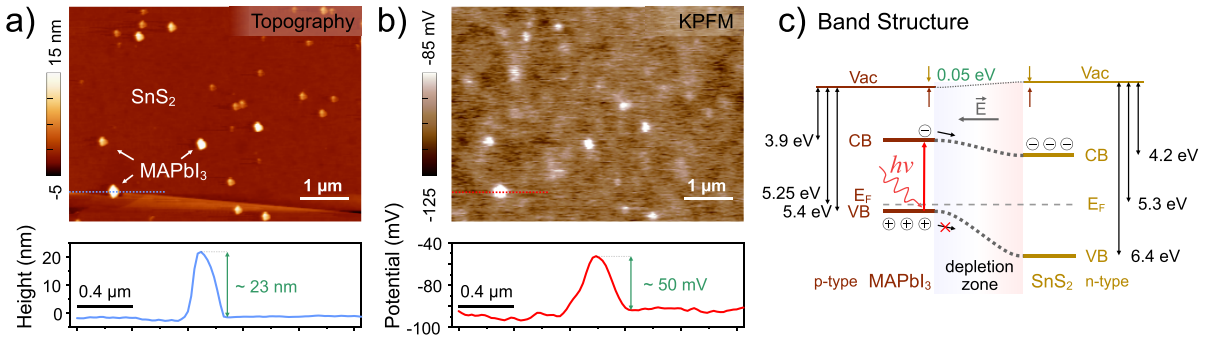


**Figure 6.** KPFM characterization of the $MAPbI_3$−$SnS_2$ heterostructure. (a) Topography image of the $MAPbI_3$ particles on $SnS_2$ flake with corresponding height profile for one of the particles. (b) KPFM image of the same area as in (a) along with the potential profile for the same particle. (c) Proposed energy level diagram of the $MAPbI_3$−$SnS_2$ heterostructure.

power: Responsivity = $(I_{DS}^{Light} - I_{DS}^{Dark})/(P_{Device})$ where $I_{DS}^{Dark}$ and $I_{DS}^{Light}$ are the same as defined above, and $P_{Device}$ is the fraction of the laser spot incident on the device channel (see details in the Supporting Information). The data in Figure 4 show that both responsivity and photoresponse are gate-voltage-dependent metrics. Responsivity is optimized while the device is in its ON state (high positive $V_G$) while the photoresponse observed in the photoswitching measurements is maximized at high negative $V_G$. The latter statement is illustrated by Figure 4d, which shows that the higher $I_{DS}^{Light}/I_{DS}^{Dark}$ ratios are observed at negative gate voltages, which explains why the data in Figure 4c,e are shown at $V_G$ = −40 V. The dependence of the photoresponse characteristics of $MAPbI_3$-decorated $SnS_2$ devices on the gate voltage provides another degree of their tunability for device applications.

Some of the functional characteristics of $MAPbI_3$-decorated $SnS_2$ FETs as potential photodetectors are illustrated by Figure 5, which presents the data collected for the device shown in Figure S2a after its modification with perovskite nanoparticles. First, we investigated the cyclability of the $MAPbI_3$-decorated $SnS_2$ FET in photoresponse measurements. Figure 5a demonstrates the results of an experiment containing more than 100 cycles of photoswitching spanning more than 10 h of continuous operation of the $MAPbI_3$-decorated $SnS_2$ device. Stable, reproducible photoresponse cycles were observed while the device was repeatedly illuminated with a green laser during this experiment, as shown in Figure 5a. A pristine $SnS_2$ device showed a similarly stable operation, although with much smaller responses, as expected (Figure S5). Furthermore, while for the $MAPbI_3$-decorated $SnS_2$ device the photocurrent changes associated with the laser turned on or off appear to be instantaneous on the time scale used in Figure 5a, a pristine


https://doi.org/10.1021/acsaelm.2c00947
ACS Appl. Electron. Mater. 2023, 5, 705−713

$SnS_2$ device exhibited a visibly slower switching kinetics (Figure S5). We further investigated the response time of the $MAPbI_3$-decorated $SnS_2$ devices to photoexcitation. The results of a typical measurement, in which we used a mechanical shutter to open and close the probe station window that was used for device illumination with a red laser, are shown in Figure 5b,c. With the characteristics of the electronics and the mechanical shutter available to us, we could study the photoresponse of $MAPbI_3$-decorated $SnS_2$ devices on the time scale of >10 ms, on which the photoswitching appeared to be instantaneous. Figure 5c shows the rise and fall response times for a typical cycle of photoresponse to a red laser of about 12 ms. It is most likely that the real photoresponse of these devices happens on a much smaller time scale and should be studied with a faster measurement setup. The functional parameters of $MAPbI_3$−$SnS_2$ photodetectors studied in this work are summarized in Table S1.

Kelvin probe force microscopy (KPFM) measurements provide evidence for the charge transfer between $MAPbI_3$ and $SnS_2$. KPFM examines the local variation of surface potential and provides a direct determination of the band offset of the $MAPbI_3$−$SnS_2$ heterostructure. We used a reference sample where freshly prepared $MAPbI_3$ solution was deposited on a few-layer $SnS_2$ flake. The thicker $SnS_2$ flake helps reduce the effect of $Si/SiO_2$ substrate on the measurements, which were performed in an inert atmosphere of nitrogen gas. A standard Pt-coated Si AFM tip was used in this study, and its work function ($W_f$) was calibrated using Au(111) test sample ($W_f$ = 5.2 eV). The topographic AFM image in Figure 6a shows the distribution of $MAPbI_3$ particles on the surface of $SnS_2$. The profile measurements indicate that the typical size of $MAPbI_3$ particles were about 10−25 nm in diameter. Figure 6b shows the corresponding KPFM image, which was measured simultaneously with the topography image. The $SnS_2$ flake has an average potential of −100 mV relative to Au(111), providing an estimate for the Fermi level ($E_f$) of $SnS_2$ flake of 5.3 eV. The KPFM image also shows bright spots in the positions corresponding to $MAPbI_3$ particles in the topography image. The potential of these particles is about 50 mV above that of the $SnS_2$ flake. Because the system is in equilibrium, the Fermi levels of $MAPbI_3$ and $SnS_2$ are the same, and the measured difference of the potentials corresponds to the difference of 0.05 eV between the vacuum levels above the studied materials. On the basis of the results of the KPFM measurements and the energies of the valence and conduction bands of $MAPbI_3$ and $SnS_2$,[3,21] we suggest a band diagram of the $MAPbI_3$−$SnS_2$ heterostructure (see Figure 6c). On the basis of the position of Fermi energy, the $MAPbI_3$ particles are p-type semiconductors, which upon contact with the n-type $SnS_2$ form a depletion zone with the electric field pointing toward $MAPbI_3$. When a $MAPbI_3$ particle absorbs a photon, it forms a pair of long-lived electron and hole with high mobility. The electric field in the depletion zone helps electrons move to the $SnS_2$ flake, while preventing the holes to do the same. As a result, illuminated $MAPbI_3$ provides additional electrons to the $SnS_2$ flake, making it more conductive as observed in our laser experiments. It should be noted again that because the $MAPbI_3$ nanoparticles did not percolate in the studied device (Figure 2f–h), the enhanced photocurrent should be due to the increased conductance of the $SnS_2$ channel. Correspondingly, Figure 6c shows that the energies of the valence and conduction bands of both materials relative to a vacuum are such that carriers excited into the conduction band of the highly absorbing $MAPbI_3$ can be transferred to the conduction band of the n-type $SnS_2$, which increases the photocurrent.[3,45] While the band diagram of the $MAPbI_3$−$SnS_2$ heterostructure in Figure 6c could be further verified by ultraviolet photoelectron spectroscopy (UPS), it appears to agree well with the experimental photoresponse data.

In summary, we demonstrate that decoration with $MAPbI_3$ perovskite nanoparticles is an efficient approach to engineer strong visible light photoresponse in electronic devices based on 2D materials with limited optical absorptivity. This approach was demonstrated using 2D $SnS_2$, a promising electronic material with a band gap of about 2.3 eV, which makes it transparent to the red region of the spectrum. FET devices based on pristine $SnS_2$ show an n-type transport with high on−off ratios. Decoration with isolated $MAPbI_3$ nanoparticles qualitatively retains the transfer characteristics of the devices but dramatically increases their photoresponse in the entire visible range of spectrum. In particular, the photoresponse of the $MAPbI_3$-decorated devices to the red light is entirely engineered by the perovskite modification of $SnS_2$, which does not absorb in the red region of spectrum. The photoresponse characteristics of the perovskite-modified $SnS_2$ devices were shown to be consistent with the intrinsic optical properties of $MAPbI_3$. The described perovskite decoration approach should be applicable to engineering photoresponse in a variety of other devices based on 2D electronic materials with low optical absorptivity.

## ■ ASSOCIATED CONTENT

### Supporting Information

The Supporting Information is available free of charge at https://pubs.acs.org/doi/10.1021/acsaelm.2c00947.

Experimental procedures; microscopic characterization of as-grown $SnS_2$ crystals (Figure S1); AFM images of pristine $SnS_2$ devices (Figure S2); XRD pattern of $MAPbI_3$ accompanied by the Rietveld analysis (Figure S3); photoresponse of a $MAPbI_3$-decorated $SnS_2$ device to lasers with different wavelengths (Figure S4); cyclic photoresponse of a pristine $SnS_2$ device to a green (517 nm) laser (Figure S5); comparison of the $MAPbI_3$-decorated $SnS_2$ devices with other photodetectors based on 2D materials reported in the literature (Table S1) (PDF)

## ■ AUTHOR INFORMATION


### Corresponding Author

**Alexander Sinitskii** − *Department of Chemistry, University of Nebraska—Lincoln, Lincoln, Nebraska 68588, United States; Nebraska Center for Materials and Nanoscience, University of Nebraska—Lincoln, Lincoln, Nebraska 68588, United States;* orcid.org/0000-0002-8688-3451; Email: sinitskii@unl.edu

### Authors

**Michael J. Loes** − *Department of Chemistry, University of Nebraska—Lincoln, Lincoln, Nebraska 68588, United States*

**Alexey Lipatov** − *Department of Chemistry, University of Nebraska—Lincoln, Lincoln, Nebraska 68588, United States; Department of Chemistry, Biology & Health Sciences and Karen M. Swindler Department of Chemical and Biological Engineering, South Dakota School of Mines and*




https://doi.org/10.1021/acsaelm.2c00947
ACS Appl. Electron. Mater. 2023, 5, 705−713

*Technology, Rapid City, South Dakota 57701, United States;* orcid.org/0000-0001-5043-1616

**Nataliia S. Vorobeva** − *Department of Chemistry, University of Nebraska—Lincoln, Lincoln, Nebraska 68588, United States*

**Haidong Lu** − *Department of Physics and Astronomy, University of Nebraska—Lincoln, Lincoln, Nebraska 68588, United States*

**Jehad Abourahma** − *Department of Chemistry, University of Nebraska—Lincoln, Lincoln, Nebraska 68588, United States*

**Dmitry S. Muratov** − *Department of Chemistry, University of Nebraska—Lincoln, Lincoln, Nebraska 68588, United States;* orcid.org/0000-0002-2027-4311

**Alexei Gruverman** − *Department of Physics and Astronomy and Nebraska Center for Materials and Nanoscience, University of Nebraska—Lincoln, Lincoln, Nebraska 68588, United States;* orcid.org/0000-0003-0492-2750

Complete contact information is available at: https://pubs.acs.org/10.1021/acsaelm.2c00947

### Author Contributions

M.J.L. prepared $SnS_2$ devices and performed their modification with perovskite nanoparticles with assistance from N.S.V. $SnS_2$ crystals were grown by D.S.M. and J.A., who also did the XRD characterization. M.J.L. performed AFM, UV−vis−NIR measurements, and Raman spectroscopy. H.L. and A.G. performed KPFM experiments and analyzed their results. M.J.L. and A.L. performed the electrical measurements. M.J.L. and A.S. wrote the manuscript. A.S. conceived the idea of this study and supervised the project.

### Notes

The authors declare no competing financial interest.

## ■ ACKNOWLEDGMENTS

The work was supported by the Nebraska Center for Energy Sciences Research (NCESR) and the National Science Foundation (NSF) through EPSCoR RII Track-1: Emergent Quantum Materials and Technologies (EQUATE), Award OIA-2044049. The device fabrication was performed using the instrumentation at the Nebraska Nanoscale Facility, which is supported by the NSF (ECCS-2025298) and the Nebraska Research Initiative.

## ■ REFERENCES

(1) Kang, S.; Lee, D.; Kim, J.; Capasso, A.; Kang, H. S.; Park, J.-W.; Lee, C.-H.; Lee, G.-H. 2D semiconducting materials for electronic and optoelectronic applications: potential and challenge. *2D Materials* **2020**, *7*, 022003.

(2) Buscema, M.; Island, J. O.; Groenendijk, D. J.; Blanter, S. I.; Steele, G. A.; van der Zant, H. S. J.; Castellanos-Gomez, A. Photocurrent generation with two-dimensional van der Waals semiconductors. *Chem. Soc. Rev.* **2015**, *44*, 3691−3718.

(3) Chen, Q.; De Marco, N.; Yang, Y.; Song, T.-B.; Chen, C.-C.; Zhao, H.; Hong, Z.; Zhou, H.; Yang, Y. Under the spotlight: The organic−inorganic hybrid halide perovskite for optoelectronic applications. *Nano Today* **2015**, *10*, 355−396.

(4) Kang, D.-H.; Pae, S. R.; Shim, J.; Yoo, G.; Jeon, J.; Leem, J. W.; Yu, J. S.; Lee, S.; Shin, B.; Park, J.-H. An Ultrahigh-Performance Photodetector based on a Perovskite-Transition-Metal-Dichalcogenide Hybrid Structure. *Adv. Mater.* **2016**, *28*, 7799−7806.

(5) Lu, J.; Carvalho, A.; Liu, H.; Lim, S. X.; Castro Neto, A. H.; Sow, C. H. Hybrid Bilayer $WSe_2$-$CH_3NH_3PbI_3$ Organolead Halide Perovskite as a High-Performance Photodetector. *Angew. Chem., Int. Ed.* **2016**, *55*, 11945−11949.

(6) Ma, C.; Shi, Y.; Hu, W.; Chiu, M. H.; Liu, Z.; Bera, A.; Li, F.; Wang, H.; Li, L. J.; Wu, T. Heterostructured $WS_2$/$CH_3NH_3PbI_3$ Photoconductors with Suppressed Dark Current and Enhanced Photodetectivity. *Adv. Mater.* **2016**, *28*, 3683−3689.

(7) Liu, F.; Wang, J.; Wang, L.; Cai, X.; Jiang, C.; Wang, G. Enhancement of photodetection based on perovskite/$MoS_2$ hybrid thin film transistor. *Journal of Semiconductors* **2017**, *38*, 034002.

(8) Wang, Y.; Fullon, R.; Acerce, M.; Petoukhoff, C. E.; Yang, J.; Chen, C.; Du, S.; Lai, S. K.; Lau, S. P.; Voiry, D.; O'Carroll, D.; Gupta, G.; Mohite, A. D.; Zhang, S.; Zhou, H.; Chhowalla, M. Solution-Processed $MoS_2$/Organolead Trihalide Perovskite Photodetectors. *Adv. Mater.* **2017**, *29*, 1603995.

(9) Bai, F.; Qi, J.; Li, F.; Fang, Y.; Han, W.; Wu, H.; Zhang, Y. A High-Performance Self-Powered Photodetector Based on Monolayer $MoS_2$/Perovskite Heterostructures. *Advanced Materials Interfaces* **2018**, *5*, 1701275.

(10) Peng, Z.-Y.; Xu, J.-L.; Zhang, J.-Y.; Gao, X.; Wang, S.-D. Solution-Processed High-Performance Hybrid Photodetectors Enhanced by Perovskite/$MoS_2$ Bulk Heterojunction. *Advanced Materials Interfaces* **2018**, *5*, 1800505.

(11) Chandrasekar, P. V.; Yang, S.; Hu, J.; Sulaman, M.; Saleem, M. I.; Tang, Y.; Jiang, Y.; Zou, B. A one-step method to synthesize $CH_3NH_3PbI_3$:$MoS_2$ nanohybrids for high-performance solution-processed photodetectors in the visible region. *Nanotechnology* **2019**, *30*, 085707.

(12) Erkılıç, U.; Solís-Fernández, P.; Ji, H. G.; Shinokita, K.; Lin, Y.-C.; Maruyama, M.; Suenaga, K.; Okada, S.; Matsuda, K.; Ago, H. Vapor Phase Selective Growth of Two-Dimensional Perovskite/$WS_2$ Heterostructures for Optoelectronic Applications. *ACS Appl. Mater. Interfaces* **2019**, *11*, 40503−40511.

(13) Yang, T.; Wang, X.; Zheng, B.; Qi, Z.; Ma, C.; Fu, Y.; Fu, Y.; Hautzinger, M. P.; Jiang, Y.; Li, Z.; Fan, P.; Li, F.; Zheng, W.; Luo, Z.; Liu, J.; Yang, B.; Chen, S.; Li, D.; Zhang, L.; Jin, S.; Pan, A. Ultrahigh-Performance Optoelectronics Demonstrated in Ultrathin Perovskite-Based Vertical Semiconductor Heterostructures. *ACS Nano* **2019**, *13*, 7996−8003.

(14) Shin, D. H.; Ko, J. S.; Kang, S. K.; Choi, S.-H. Enhanced Flexibility and Stability in Perovskite Photodiode−Solar Cell Nanosystem Using $MoS_2$ Electron-Transport Layer. *ACS Appl. Mater. Interfaces* **2020**, *12*, 4586−4593.

(15) Wang, H.; Wang, X.; Chen, Y.; Zhang, S.; Jiang, W.; Zhang, X.; Qin, J.; Wang, J.; Li, X.; Pan, Y.; Liu, F.; Shi, Z.; Zhang, H.; Tu, L.; Wang, H.; Long, H.; Li, D.; Lin, T.; Wang, J.; Zhan, Y.; Shen, H.; Meng, X.; Chu, J. Extremely Low Dark Current $MoS_2$ Photodetector via 2D Halide Perovskite as the Electron Reservoir. *Adv. Opt. Mater.* **2020**, *8*, 1901402.

(16) Muratov, D. S.; Ishteev, A. R.; Lypenko, D. A.; Vanyushin, V. O.; Gostishev, P.; Perova, S.; Saranin, D. S.; Rossi, D.; Auf der Maur, M.; Volonakis, G.; Giustino, F.; Persson, P. O. Å.; Kuznetsov, D. V.; Sinitskii, A.; Di Carlo, A. Slot-Die-Printed Two-Dimensional $ZrS_3$ Charge Transport Layer for Perovskite Light-Emitting Diodes. *ACS Appl. Mater. Interfaces* **2019**, *11*, 48021−48028.

(17) Agresti, A.; Pazniak, A.; Pescetelli, S.; Di Vito, A.; Rossi, D.; Pecchia, A.; Auf der Maur, M.; Liedl, A.; Larciprete, R.; Kuznetsov, D. V.; Saranin, D.; Di Carlo, A. Titanium-carbide MXenes for work function and interface engineering in perovskite solar cells. *Nat. Mater.* **2019**, *18*, 1228−1234.

(18) Wang, Q. H.; Kalantar-Zadeh, K.; Kis, A.; Coleman, J. N.; Strano, M. S. Electronics and optoelectronics of two-dimensional transition metal dichalcogenides. *Nat. Nanotechnol.* **2012**, *7*, 699−712.

(19) Jariwala, D.; Sangwan, V. K.; Lauhon, L. J.; Marks, T. J.; Hersam, M. C. Emerging Device Applications for Semiconducting Two-Dimensional Transition Metal Dichalcogenides. *ACS Nano* **2014**, *8*, 1102−1120.

(20) Huang, Y.; Sutter, E.; Sadowski, J. T.; Cotlet, M.; Monti, O. L. A.; Racke, D. A.; Neupane, M. R.; Wickramaratne, D.; Lake, R. K.; Parkinson, B. A.; Sutter, P. Tin Disulfide—An Emerging Layered Metal Dichalcogenide Semiconductor: Materials Properties and Device Characteristics. *ACS Nano* **2014**, *8*, 10743−10755.

(21) Burton, L. A.; Whittles, T. J.; Hesp, D.; Linhart, W. M.; Skelton, J. M.; Hou, B.; Webster, R. F.; O'Dowd, G.; Reece, C.; Cherns, D.; Fermin, D. J.; Veal, T. D.; Dhanak, V. R.; Walsh, A. Electronic and optical properties of single crystal $SnS_2$: an earth-abundant disulfide photocatalyst. *J. Mater. Chem. A* **2016**, *4*, 1312−1318.
(22) Wei, S.; Ge, C.; Zhou, L.; Zhang, S.; Dai, M.; Gao, F.; Sun, Y.; Qiu, Y.; Wang, Z.; Zhang, J.; Hu, P. Performance Improvement of Multilayered $SnS_2$ Field Effect Transistors through Synergistic Effect of Vacancy Repairing and Electron Doping Introduced by EDTA. *ACS Appl. Electron. Mater.* **2019**, *1*, 2380−2388.
(23) Wang, Y.; Huang, L.; Wei, Z. Photoresponsive field-effect transistors based on multilayer $SnS_2$ nanosheets. *Journal of Semiconductors* **2017**, *38*, 034001.
(24) Sriv, T.; Kim, K.; Cheong, H. Low-Frequency Raman Spectroscopy of Few-Layer 2H-$SnS_2$. *Sci. Rep.* **2018**, *8*, 10194.
(25) Fan, C.; Li, Y.; Lu, F.; Deng, H.-X.; Wei, Z.; Li, J. Wavelength dependent UV-Vis photodetectors from $SnS_2$ flakes. *RSC Adv.* **2016**, *6*, 422−427.
(26) Zschieschang, U.; Holzmann, T.; Kuhn, A.; Aghamohammadi, M.; Lotsch, B. V.; Klauk, H. Threshold-voltage control and enhancement-mode characteristics in multilayer tin disulfide field-effect transistors by gate-oxide passivation with an alkylphosphonic acid self-assembled monolayer. *J. Appl. Phys.* **2015**, *117*, 104509.
(27) Chu, D.; Pak, S. W.; Kim, E. K. Locally Gated $SnS_2$/hBN Thin Film Transistors with a Broadband Photoresponse. *Sci. Rep.* **2018**, *8*, 10585.
(28) Lipatov, A.; Wilson, P. M.; Shekhirev, M.; Teeter, J. D.; Netusil, R.; Sinitskii, A. Few-layered titanium trisulfide ($TiS_3$) field-effect transistors. *Nanoscale* **2015**, *7*, 12291−12296.
(29) Choi, Y. C.; Lee, S. W.; Kim, D.-H. Antisolvent-assisted powder engineering for controlled growth of hybrid $CH_3NH_3PbI_3$ perovskite thin films. *APL Materials* **2017**, *5*, 026101.
(30) Zobel, A.; Boson, A.; Wilson, P. M.; Muratov, D. S.; Kuznetsov, D. V.; Sinitskii, A. Chemical vapour deposition and characterization of uniform bilayer and trilayer $MoS_2$ crystals. *J. Mater. Chem. C* **2016**, *4*, 11081−11087.
(31) Lipatov, A.; Li, T.; Vorobeva, N. S.; Sinitskii, A.; Gruverman, A. Nanodomain Engineering for Programmable Ferroelectric Devices. *Nano Lett.* **2019**, *19*, 3194−3198.
(32) Troughton, J.; Hooper, K.; Watson, T. M. Humidity resistant fabrication of $CH_3NH_3PbI_3$ perovskite solar cells and modules. *Nano Energy* **2017**, *39*, 60−68.
(33) Boix, P. P.; Agarwala, S.; Koh, T. M.; Mathews, N.; Mhaisalkar, S. G. Perovskite Solar Cells: Beyond Methylammonium Lead Iodide. *J. Phys. Chem. Lett.* **2015**, *6*, 898−907.
(34) Huang, J.; Yuan, Y.; Shao, Y.; Yan, Y. Understanding the physical properties of hybrid perovskites for photovoltaic applications. *Nat. Rev. Mater.* **2017**, *2*, 17042.
(35) Xie, C.; Mak, C.; Tao, X.; Yan, F. Photodetectors Based on Two-Dimensional Layered Materials Beyond Graphene. *Adv. Funct. Mater.* **2017**, *27*, 1603886.
(36) Lin, J.; Li, H.; Zhang, H.; Chen, W. Plasmonic enhancement of photocurrent in $MoS_2$ field-effect-transistor. *Appl. Phys. Lett.* **2013**, *102*, 203109.
(37) Britnell, L.; Ribeiro, R. M.; Eckmann, A.; Jalil, R.; Belle, B. D.; Mishchenko, A.; Kim, Y.-J.; Gorbachev, R. V.; Georgiou, T.; Morozov, S. V.; Grigorenko, A. N.; Geim, A. K.; Casiraghi, C.; Neto, A. H. C.; Novoselov, K. S. Strong Light-Matter Interactions in Heterostructures of Atomically Thin Films. *Science* **2013**, *340*, 1311−1314.
(38) Sinitskii, A.; Dimiev, A.; Kosynkin, D. V.; Tour, J. M. Graphene Nanoribbon Devices Produced by Oxidative Unzipping of Carbon Nanotubes. *ACS Nano* **2010**, *4*, 5405−5413.
(39) Deretzis, I.; Alberti, A.; Pellegrino, G.; Smecca, E.; Giannazzo, F.; Sakai, N.; Miyasaka, T.; La Magna, A. Atomistic origins of $CH_3NH_3PbI_3$ degradation to $PbI_2$ in vacuum. *Appl. Phys. Lett.* **2015**, *106*, 131904.
(40) Vorobeva, N. S.; Bagheri, S.; Torres, A.; Sinitskii, A. Negative photoresponse in $Ti_3C_2T_x$ MXene monolayers. *Nanophotonics* **2022**, *11*, 3953−3960.
(41) Vorobeva, N. S.; Lipatov, A.; Torres, A.; Dai, J.; Abourahma, J.; Le, D.; Dhingra, A.; Gilbert, S. J.; Galiy, P. V.; Nenchuk, T. M.; Muratov, D. S.; Rahman, T. S.; Zeng, X. C.; Dowben, P. A.; Sinitskii, A. Anisotropic Properties of Quasi-1D $In_4Se_3$: Mechanical Exfoliation, Electronic Transport, and Polarization-Dependent Photoresponse. *Adv. Funct. Mater.* **2021**, *31*, 2106459.
(42) Lipatov, A.; Vorobeva, N. S.; Li, T.; Gruverman, A.; Sinitskii, A. Using Light for Better Programming of Ferroelectric Devices: Optoelectronic $MoS_2$-Pb(Zr,Ti)$O_3$ Memories with Improved On−Off Ratios. *Adv. Electron. Mater.* **2021**, *7*, 2001223.
(43) Wu, J.-J.; Tao, Y.-R.; Wu, Y.; Wu, X.-C. Ultrathin $SnS_2$ nanosheets of ultrasonic synthesis and their photoresponses from ultraviolet to near-infrared. *Sens. Actuators, B* **2016**, *231*, 211−217.
(44) Huang, Y.; Deng, H.-X.; Xu, K.; Wang, Z.-X.; Wang, Q.-S.; Wang, F.-M.; Wang, F.; Zhan, X.-Y.; Li, S.-S.; Luo, J.-W.; He, J. Highly sensitive and fast phototransistor based on large size CVD-grown $SnS_2$ nanosheets. *Nanoscale* **2015**, *7*, 14093−14099.
(45) Im, H. S.; Myung, Y.; Cho, Y. J.; Kim, C. H.; Kim, H. S.; Back, S. H.; Jung, C. S.; Jang, D. M.; Lim, Y. R.; Park, J.; Ahn, J.-P. Facile phase and composition tuned synthesis of tin chalcogenide nanocrystals. *RSC Adv.* **2013**, *3*, 10349−10354.




https://doi.org/10.1021/acsaelm.2c00947
*ACS Appl. Electron. Mater.* 2023, 5, 705−713